Meas. Sci. Technol. **18** (2007) 3144–3154 doi:10.1088/0957-0233/18/10/S16

Behaviour of intrinsic polymer optical fibre sensor for large-strain applications

Sharon Kiesel[1], **Kara Peters**[1], **Tasnim Hassan**[2] **and Mervyn Kowalsky**[2]

[1] Department of Mechanical and Aerospace Engineering, North Carolina State University, Campus Box 7910, Raleigh, NC 27695, USA
[2] Department of Civil, Construction and Environmental Engineering, North Carolina State University, Campus Box 7908, Raleigh, NC 27695, USA

E-mail: kjpeters@eos.ncsu.edu

Received 31 December 2006, in final form 23 February 2007
Published 12 September 2007
Online at stacks.iop.org/MST/18/3144

Abstract
This paper derives the phase response of a single-mode polymer optical fibre for large-strain applications. The role of the finite deformation of the optical fibre and nonlinear strain optic effects are derived using a second order strain assumption and shown to be important at strain magnitudes as small as 1%. In addition, the role of the core radius change on the propagation constant is derived, but it is shown to be negligible as compared to the previous effects. It is shown that four mechanical and six opto-mechanical parameters must be calibrated to apply the sensor under arbitrary axial and transverse loading. The mechanical nonlinearity of a typical single-mode polymer optical fibre is experimentally measured in axial tension and is shown to be more significant than that of their silica counterpart. The mechanical parameters of the single-mode polymer optical fibre are also measured for a variety of strain rates, from which it is demonstrated that the strain rate has a strong influence on yield stress and strain. The calibrated constants themselves are less affected by strain rate.

Keywords: large strain, polymer optical fibre, optical fibre sensor

(Some figures in this article are in colour only in the electronic version)

1. Introduction

Intrinsic polymer optical fibre (POF) sensors have great potential for large-strain applications such as health monitoring of civil infrastructure systems subjected to earthquake loading or structures with large shape changes such as morphing aircraft [1, 2]. POFs provide a large elastic strain range, are more flexible than silica optical fibres, and are more durable in harsh chemical or environmental conditions. Xiong *et al* demonstrated 6% strain before failure of a POF and cites a potential 13% increase with the improvement of manufacturing techniques [3]. Thus, for structural health monitoring applications, POF sensor systems potentially offer a larger strain range measurement capability along with more long-term survivability. While POF sensors have been used considerably for chemical and environmental monitoring due to the high sensitivity of polymers to environmental factors, only recently has their use in the monitoring of mechanical properties been explored.

Kuang *et al* [4, 5] applied surface mounted, multi-mode POFs to detect cracks and monitor deflection in concrete beams. The principle of the intensity-based measurement applied by [4, 5] was decreased internal reflection due to fibre bending. The greater flexibility of the POF as compared to silica optical fibres allows larger curvatures before failure of the sensor. To further increase the sensitivity of the measurements, the POF (of 1 mm diameter) was etched to increase the loss in mode propagation due to bending. A similar concept was applied by Takeda for POFs embedded in a laminated composite [6]. Later, Kuang and Cantwell successfully applied the intensity-based POF sensor to measure the dynamic response of undamaged and damaged laminated composite beams [7].

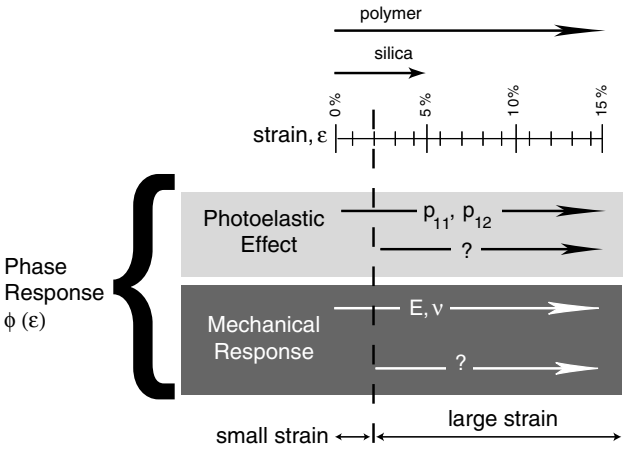

Figure 1. Schematic diagram of contributions to phase shift of a lightwave propagating through an optical fibre for an applied axial strain range of $0\% < \epsilon < 15\%$. Required coefficients to be calibrated are divided into two categories: photoelastic and mechanical. Known coefficients are given whereas unknown coefficients are indicated by '?'. Division point between small and large strain regions is arbitrary for this diagram.

Intensity-based measurements, however, are limited in application due to the presence of multiple modes propagating through the optical fibre and therefore produce lower measurement accuracy and resolution [8]. Recent advances in the fabrication of single-mode POFs have made it possible to extend POFs to interferometric sensing. Silva-Lopez *et al* [2] measured the strain and temperature sensitivity of a single-mode PMMA POF at 632.8 nm to be $\mathrm{d}\varphi/\mathrm{d}L = 131 \times 10^5$ rad m^{-1}, consistent with the value for bulk PMMA. However, this strain sensitivity was measured for a strain range of 0–0.04%, well below that at which the strain sensor would typically be applied. The goal of this paper is to predict the behaviour of the POF for large strain applications and derive the associated phase shift of an intrinsic POF sensor.

The standard description of the sensitivity of an intrinsic optical fibre sensor to applied strain is written in the form

$$\Delta\varphi = \left(\frac{\mathrm{d}\varphi}{\mathrm{d}\epsilon}\right)\epsilon, \tag{1}$$

where ϵ is the applied strain field and $\Delta\varphi$ is the change in phase shift of a lightwave propagating through the optical fibre [9]. Equation (1) is applicable when the magnitude of the strain component is small ($\epsilon \ll 1$) such that the effect of applied strain can be linearized about $\epsilon = 0$. However, in general if we allow ϵ to be of arbitrary magnitude ($\epsilon < 1$), we can write

$$\Delta\varphi = \left(\frac{\mathrm{d}\varphi}{\mathrm{d}\epsilon}\right)\epsilon + \frac{1}{2}\left(\frac{\mathrm{d}^2\varphi}{\mathrm{d}\epsilon^2}\right)\epsilon^2 + \frac{1}{6}\left(\frac{\mathrm{d}^3\varphi}{\mathrm{d}\epsilon^3}\right)\epsilon^3 + \cdots, \tag{2}$$

where the number of terms required depends upon the magnitude of ϵ.

A schematic of the contributions to $\Delta\varphi$ is shown in figure 1. The optical path length of a lightwave propagating through the optical fibre, φ is altered by the load applied to the optical fibre through two effects: the change in index of refraction of the optical medium and the change in length of the medium. These can be written in terms of two separate sets of material properties: the photoelastic coefficients and mechanical coefficients. In the strain region for which the phase response to applied load is linear (i.e. where (1) is applicable), the number of required properties to describe the phase shift of the propagating lightwave is well known. Assuming the material is isotropic, two independent photoelastic and two independent mechanical coefficients are required. At a certain magnitude of strain, this description is not sufficient and therefore the second term of (2) is required. At this point further photoelastic and mechanical coefficients are required. These coefficients have not yet been identified and are therefore indicated by question marks in figure 1. One could expand figure 1 to larger magnitudes of strain and therefore a higher number of terms from (2), however, the second order term will be sufficient for this paper.

Potential effects contributing to the term $(\mathrm{d}^2\varphi/\mathrm{d}\epsilon^2)\epsilon^2$ of (2) include the (1) finite deformation of the POF and (2) nonlinear strain optic effects in the polymer. Bertholds and Dandliker [10] recognized the importance of including second order strain terms (ϵ^2) even for silica fibres near failure strains. Additionally, Kuang *et al* [4] observed necking and whitening of the POF at the location of the highest strain, indicating large, local finite deformation of the POF. The exact value of strain at which these are required will vary from material to material. Approximate strain ranges for both silica and polymer optical fibres have also been included in figure 1 although this will be discussed in more detail later. The important concept to understand from the schematic of figure 1 is that unless the magnitudes of each of the required photoelastic and mechanical coefficients are known, their relative importance in the calculation of the phase response for a given value of φ is not known. In other words, one cannot *a priori* neglect either of these effects until they have both been measured. Additionally, while axial loading is the most common applied to such sensors, this may not be a sufficient loading case for calibration purposes. Instead several of the independent coefficients must be determined if the sensor is to be subjected to an arbitrary loading in the future.

The role of the finite deformation and the nonlinear strain-optic effect will be analysed in this paper, following a derivation that is consistent in the order of applied strain (second order). To accomplish this, we must also identify the material properties (in this case both mechanical and opto-mechanical) that must be calibrated for the POF sensor for large strain applications and the minimum strain value for which the nonlinearities must be considered for accurate interpretation of the applied strain. It will be demonstrated that a total of four mechanical and six opto-mechanical coefficients must be known to characterize the response of the intrinsic sensor. This formulation would also be applicable to the calculation of the wavelength shifts in fibre Bragg gratings in POF fibres [3]. Following the derivations, this paper presents the results of mechanical testing of a typical single-mode polymer optical fibre including the nonlinear behaviour, the yield stress and strain, and effects of strain rate on these properties. The measured mechanical properties are then applied to the derived sensor response formulation to demonstrate the increased importance of including the mechanical nonlinearities as compared to silica optical fibres. Measurements of the photoelastic properties of the POF and their relative importance in the formulation are not included due to space constraints, but will be investigated thoroughly in a future paper.

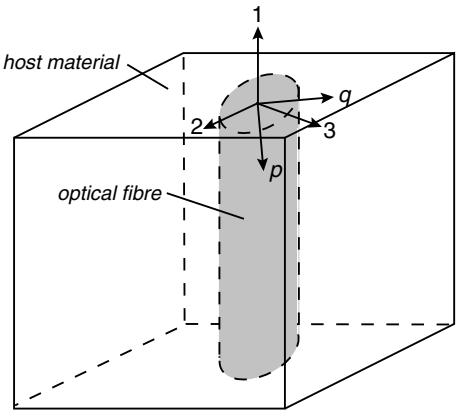

Figure 2. Coordinate system for optical fibre sensor.

2. Analysis

We consider the optical fibre to be mechanically and optically isotropic [9]. In general, the fibre can be surface mounted or embedded with any combination of applied strain fields therefore we need to be able to predict its response for any such strain fields. For this derivation, we consider that the strain field is constant along the fibre; however, for a varying strain field along the fibre the change in phase can be integrated along the fibre [11]. The optical fibre considered and its coordinate system are shown in figure 2. The 1–2–3 coordinate system are the directions of applied strain as shown. The *p*–*q* axes are in the optical principal directions of the fibre cross-section which coincide with the principal strain directions in the 2–3 plane for an initially isotropic fibre. Thus, the *p*–*q* axes rotate with the applied strain field. The phase shift of a lightwave propagating through the optical fibre is given by

$$\varphi = \beta L, \tag{3}$$

where β is the propagation constant and L is the length of the optical fibre [12]. For a single-mode fibre, we consider only the value of β for the fundamental core mode. β can be written in terms of the effective index of refraction of the fundamental core mode, n_e,

$$\beta = n_e \frac{2\pi}{\lambda}, \tag{4}$$

where λ is the wavelength of the propagating light. Once a strain field is applied to the optical fibre, the change in phase shift due to the applied strain can be written as

$$\Delta\varphi = \Delta\beta L + \Delta L\beta = \Delta\beta L + \beta L\epsilon_1 = \frac{2\pi}{\lambda} L(\Delta n_e + \epsilon_1 n_e), \tag{5}$$

where ϵ_1 is the strain in the axial direction. The change Δn_e has two components, one due to the change in diameter of the fibre core, the second due to the photo-elastic effect. The second term is derived here, whereas the first term is discussed in section 4.

2.1. Opto-mechanical response

The index of refraction experienced by light propagating through the fibre in the 1 direction can be written in terms of the components of the material dielectric tensor **B** [9]

$$\frac{1}{n_e^2} = \frac{(B_2 + B_3) \pm \sqrt{(B_2 - B_3)^2 + 4B_4^2}}{2}. \tag{6}$$

For an isotropic material, these terms are simply given as $B_1 = B_2 = B_3 = 1/n_0^2$, and $B_4 = B_5 = B_6 = 0$, where n_0 is the effective index of refraction of the unloaded fibre in the 1 direction. The optical fibre is essentially assumed to be a homogeneous, isotropic material with an initial effective index of refraction n_0. In order to calculate the $\Delta n = n_e - n_0$ due to applied strain, we write $B_i = B_i^0 + \Delta B_i$, yielding the index of refraction after applied strain as

$$\frac{1}{n_e^2} = \frac{1}{n_0^2} + \frac{(\Delta B_2 + \Delta B_3) \pm \sqrt{(\Delta B_2 - \Delta B_3)^2 + 4\Delta B_4^2}}{2}. \tag{7}$$

We then write the change in index of refraction due to multiple strain components through the strain-optic effect including orders ϵ and ϵ^2,

$$\Delta B_m = p_{mn}\epsilon_n + g_{mlk}\epsilon_k\epsilon_l, \tag{8}$$

where the strain components are given in compact notation (i.e., $\epsilon_1 = \epsilon_{11}, \epsilon_2 = \epsilon_{22}, \epsilon_3 = \epsilon_{33}, \epsilon_4 = \epsilon_{23}, \epsilon_5 = \epsilon_{13}, \epsilon_6 = \epsilon_{12}$) and the summation notation is implied [13]. For an initially isotropic material, the components of the linear strain-optic tensor, **p**, are given in terms of two constants p_{11} and p_{12} [13]:

$$\mathbf{p} = \begin{bmatrix} p_{11} & p_{12} & p_{12} & 0 & 0 & 0 \\ p_{12} & p_{11} & p_{12} & 0 & 0 & 0 \\ p_{12} & p_{12} & p_{11} & 0 & 0 & 0 \\ 0 & 0 & 0 & \frac{(p_{11}-p_{12})}{2} & 0 & 0 \\ 0 & 0 & 0 & 0 & \frac{(p_{11}-p_{12})}{2} & 0 \\ 0 & 0 & 0 & 0 & 0 & \frac{(p_{11}-p_{12})}{2} \end{bmatrix}. \tag{9}$$

In this paper we introduce the tensor **g** of dimension three in (8) to represent the nonlinear term of the strain-optic effect. As for the linear strain-optic effect, (8) can be written either in terms of stress or strain. For small deformations, a simple relationship between the photoelastic tensor **p** and its equivalent for the stress-optic effect exist [13]. However, for large deformations, the relationship between **g** and its equivalent for the nonlinear stress-optic effect depends upon the particular state of stress and therefore the two formulations are not easily interchangeable. For this work, we consider the strain formulation of (8) since displacement compatibility is typically enforced between the sensor and the surrounding medium in which it is embedded.

Since our goal is to predict the opto-mechanical response of the sensor, we must first identify the number of independent material constants appearing in (8) in addition to p_{11} and p_{12}. We first reduce the number of unknowns through the symmetry condition, $g_{mlk} = g_{mkl}$. Second, applying isotropic material properties and uncoupling the effects of normal and shear strains reduces the number of independent constants in **g** to four ($g_{111}, g_{112}, g_{122}, g_{123}$) [14]. This approximation is only valid for deformations without significant shear strains; however this is a reasonable assumption for most strain sensor applications since shear strains do not transfer well to the optical fibre. The non-zero components of **g** are listed in table 1 in terms of these four independent constants.

Table 1. Non-zero components of the non-linear photoelastic tensor **g**. Additional terms appear for components $g_1 \ldots$; however these are not required for (7), therefore they are not included here.

Component	Value
g_{211}	g_{122}
g_{212}, g_{221}	g_{112}
g_{213}, g_{231}	g_{123}
g_{222}	g_{111}
g_{233}	g_{122}
g_{244}	$(g_{111} - 2g_{112} + g_{122})/4$
g_{255}	$(g_{122} - g_{123})/2$
g_{266}	$(g_{111} - 2g_{112} + g_{122})/4$
g_{311}	g_{122}
g_{312}, g_{321}	g_{123}
g_{313}, g_{331}	g_{112}
g_{322}	g_{112}
g_{333}	g_{111}
g_{344}	$(g_{111} - 2g_{112} + g_{122})/4$
g_{355}	$(g_{111} - 2g_{112} + g_{122})/4$
g_{366}	$g_{122} - g_{123})/2$
g_{414}, g_{441}	$(g_{112} - g_{123})/2$
g_{424}, g_{442}	$(g_{111} - g_{122})/4$
g_{343}, g_{443}	$(g_{111} - g_{122})/4$
g_{456}, g_{465}	$(g_{111} - 2g_{112} - g_{122} + 2g_{123})/8$

Including shear strain would significantly increase the complexity of the calibrations required. For the case of pure applied torsion in the 2–3 plane, one could apply the finite deformation solution of [15] for the torsion of a circular cylinder including nonlinear photoelastic effects. For brevity, this solution is not listed here. Instead, we point out that the finite elasticity solution differs from the linear elastic solution in that (1) a third mechanical nonlinearity constant appears in addition to the two to be introduced in section 2.2; (2) the deformation in the radial direction is inhomogeneous which may limit the assumption of uniform strain throughout the cross-section; and (3) there is a significant change in core diameter due to the torsional load.

Expanding (8) in terms of the components of **p** and **g** yields the required dielectric tensor changes for (7),

$$\begin{aligned}\Delta B_2 + \Delta B_3 &= 2p_{12}\epsilon_1 + 2g_{122}\epsilon_1^2 + 4g_{112}\epsilon_2\epsilon_3 + (g_{111} + g_{122})\left(\epsilon_2^2 + \epsilon_3^2\right) \\ &\quad + [p_{11} + p_{12} + 2\epsilon_1(g_{123} + g_{112})](\epsilon_2 + \epsilon_3) \\ &\quad + \tfrac{1}{4}(g_{111} - 2g_{112} + g_{122})\left(2\epsilon_4^2 + \epsilon_5^2 + \epsilon_6^2\right) \\ &\quad + \tfrac{1}{2}(g_{122} - g_{123})\left(\epsilon_5^2 + \epsilon_6^2\right) \qquad (10)\end{aligned}$$

$$\begin{aligned}\Delta B_2 - \Delta B_3 &= [p_{11} - p_{12} + 2\epsilon_1(g_{112} - g_{123})](\epsilon_2 - \epsilon_3) \\ &\quad + (g_{111} - g_{122})\left(\epsilon_2^2 - \epsilon_3^2\right) \\ &\quad + \tfrac{1}{4}(-g_{111} + 2g_{112} + g_{122} - 2g_{123})\left(\epsilon_5^2 - \epsilon_6^2\right) \qquad (11)\end{aligned}$$

$$\begin{aligned}\Delta B_4 &= \tfrac{1}{2}(p_{11} - p_{12})\epsilon_4 + (g_{111} - g_{122})\epsilon_1\epsilon_4 \\ &\quad + \tfrac{1}{2}(g_{111} - g_{122})(\epsilon_2\epsilon_4 + \epsilon_3\epsilon_4) \\ &\quad + \tfrac{1}{4}(g_{111} - 2g_{112} - g_{122} + 2g_{123})\epsilon_5\epsilon_6. \qquad (12)\end{aligned}$$

Further reducing (10)–(12) to the case without shear strain,

$$\begin{aligned}\Delta B_2 + \Delta B_3 &= 2p_{12}\epsilon_1 + 2g_{122}\epsilon_1^2 + 4g_{112}\epsilon_2\epsilon_3 \\ &\quad + [p_{11} + p_{12} + 2\epsilon_1(g_{123} + g_{112})](\epsilon_2 + \epsilon_3) \\ &\quad + (g_{111} + g_{122})\left(\epsilon_2^2 + \epsilon_3^2\right)\end{aligned}$$

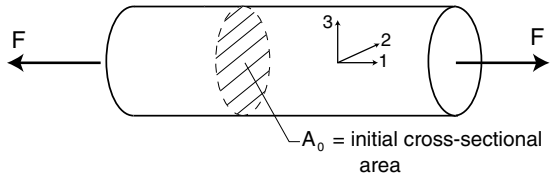

Figure 3. Axial loading condition for optical fibre.

$$\begin{aligned}&= [p_{11} - p_{12} + 2\epsilon_1(g_{112} - g_{123})](\epsilon_2 - \epsilon_3) \\ &\quad + (g_{111} - g_{122})\left(\epsilon_2^2 - \epsilon_3^2\right) \\ \Delta B_4 &= 0. \qquad (13)\end{aligned}$$

2.2. *Mechanical deformation of optical fibre*

Having derived an expression for the phase shift in an optical fibre as a function of applied strain, we now derive the strain components for both axial and transverse loading to the optical fibre.

2.2.1. Axial loading. The role of the finite deformation of the optical fibre at large strain values for the case of axial tension was demonstrated by Bertholds and Dandliker [10] and Nellen *et al* [16]. Both measured a quadratic form of the opto-mechanical response of the fibre with applied axial stress and associated this behaviour with the finite deformation of the fibre cross-section. Each of these experiments were performed with silica optical fibres which are considerably more brittle than the POF and fail at strain levels below 5%. Therefore, one expects the role of the finite deformation of the optical fibre to increase for the POF at high-strain magnitudes.

Since the most common loading case for calibration experiments is pure axial loading of the optical fibre, as seen in figure 3, we first derive the phase shift in the POF for this case. From [10] the longitudinal and transverse elongations can be written as

$$\epsilon_l = \epsilon + \delta\epsilon^2 \qquad \epsilon_t = -\nu\epsilon + \alpha\epsilon^2 \qquad \epsilon = F/(E_0 A_0)\,, \quad (14)$$

where F is the applied axial force, A_0 is the initial cross-sectional area of the fibre and E_0 is the initial Young's modulus of the fibre at small strains. δ and α are defined as the nonlinearity constants in the longitudinal and transverse elongations, respectively. From these elongations, one can solve for the strain components

$$\begin{aligned}\epsilon_1 &= \epsilon_l + \frac{1}{2}\epsilon^2 \\ \epsilon_2 = \epsilon_3 &= \epsilon_t + \frac{\nu^2}{2}\epsilon^2 \qquad (15) \\ \epsilon_4 = \epsilon_5 &= \epsilon_6 = 0.\end{aligned}$$

Substituting (15) into (10)–(12) into (7) yields the index of refraction change in the POF as a function of strain. From this expression for n_e, the phase shift in the POF can be found using (5). For the POF at large strain values, one cannot linearize the phase shift sensitivity as in previous derivations for silica fibres (see for example [9]). However, in order to fit later experimental data, we expand $\Delta\varphi$ as a Taylor series

about $\epsilon = 0$,

$$\Delta\varphi(\epsilon) = \Delta\varphi\Big|_{\epsilon=0} + \left(\frac{\mathrm{d}\varphi}{\mathrm{d}\epsilon}\right)\Big|_{\epsilon=0}\epsilon + \left(\frac{\mathrm{d}^2\varphi}{\mathrm{d}\epsilon^2}\right)\Big|_{\epsilon=0}\frac{\epsilon^2}{2} + O(\epsilon^3)$$
$$\approx \left(\frac{\mathrm{d}\varphi}{\mathrm{d}\epsilon}\right)\Big|_{\epsilon=0}\epsilon + \left(\frac{\mathrm{d}^2\varphi}{\mathrm{d}\epsilon^2}\right)\Big|_{\epsilon=0}\frac{\epsilon^2}{2}. \tag{16}$$

Knowing that $\Delta\varphi = 0$ at $\epsilon = 0$ and neglecting terms of at least $O(\epsilon^3)$, we find the linear and nonlinear strain sensitivities for use in (2),

$$\frac{\mathrm{d}\varphi}{\mathrm{d}\epsilon} = \frac{2\pi}{\lambda}Ln_0\left[1 - \frac{n_0^2}{2}\left(p_{12} - \nu(p_{11} + p_{12})\right)\right]$$
$$\frac{\mathrm{d}^2\varphi}{\mathrm{d}\epsilon^2} = \frac{\pi}{\lambda}Ln_0\left[\delta - \frac{n_0^2}{2}\left(\left(\delta + \frac{1}{2}\right)p_{12} + \left(\alpha + \frac{\nu^2}{2}\right)(p_{11} + p_{12})\right.\right.$$
$$\left.\left. + 2\nu(g_{112} + g_{123}) - g_{122} - \nu^2(g_{111} + 2g_{112} + g_{122})\right)\right]. \tag{17}$$

The linear term of (17) is the same used for the fibre at small strains [9, 12]. The second order term includes the terms derived by [10] accounting for the finite deformation of the optical fibre as well as additional terms accounting for the nonlinear photoelastic effect. The relative magnitude of these terms in $\mathrm{d}^2\varphi/\mathrm{d}\epsilon^2$ cannot be known *a priori* until the nonlinear material parameters δ, α and $\mathbf{g}$ are known for the POF.

As mentioned in the previous section, n_e also changes due to the photoelastic effect derived above as well as the change in core radius, a. The change in index of refraction due to the change in core radius can be written as $(\mathrm{d}n_e/\mathrm{d}a)(\mathrm{d}a/\mathrm{d}\epsilon)\epsilon$. In order to estimate the term $\mathrm{d}a/\mathrm{d}\epsilon$ for the axial loading case of figure 3, we approximate the radius of the optical fibre core after applied strain as

$$a = a_0(1 + \epsilon_t) = a_0(1 - \nu\epsilon + \alpha\epsilon^2), \tag{18}$$

where a_0 is the radius of the undeformed core. Therefore

$$\frac{\mathrm{d}a}{\mathrm{d}\epsilon_0} = a_0(-\nu + 2\alpha\epsilon). \tag{19}$$

To estimate the term $\mathrm{d}n_e/\mathrm{d}a$, we apply the approximate expression for the normalized phase constant b found in [22]

$$b = \frac{n_e - n_2}{n_1 - n_2} \approx \frac{(1.1428V - 0.9960)^2}{V^2} \tag{20}$$

with $V = (2a\pi/\lambda)\sqrt{n_1^2 - n_2^2}$ where n_1 and n_2 are the index of refraction of the core and cladding optical fibre materials, respectively. Rewriting (20) in terms of n_e and taking the derivative with respect to a, we find

$$\frac{\mathrm{d}n_e}{\mathrm{d}a} \approx \frac{\lambda}{2\pi a_0^2}\sqrt{\frac{n_1 - n_2}{n_1 + n_2}}\left[-1.306V + 3.415 - \frac{1.984}{V}\right]. \tag{21}$$

2.2.2. Transverse loading. Second, we consider the case of transverse normal stress applied to the optical fibre, as shown in figure 4(*a*), important for a sensor embedded in a host material. The direction of applied transverse stress does not affect the phase shift in the fibre, therefore we arbitrarily consider that is applied along the 3-axis. While an exact solution is known for the strain field during small strain deformation of the circular cross-section of the optical fibre, the domain of large strain

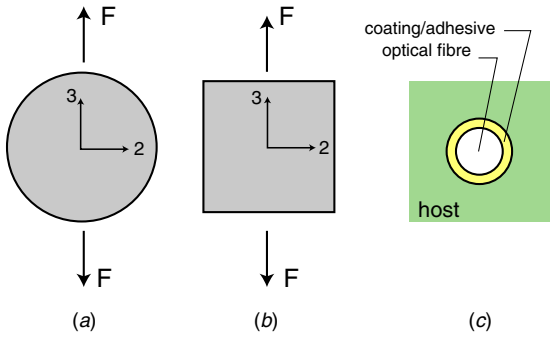

Figure 4. Transverse loading on optical fibre. (*a*) Actual fibre geometry; (*b*) assumed fibre geometry; (*c*) embedded fibre with coating in host material.

requires a more complex numerical solution [17]. The purpose of this paper is to determine the relative magnitude of different effects when the POF is subjected to large strains, therefore we consider the simplified problem of a square cross-section of equivalent area shown in figure 4(*b*). The presence of a coating surrounding the sensor (figure 4(*c*)) would further reduce the stress concentration at the centre of the fibre. The resulting strain field is simply a rotation of the axial loading case

$$\epsilon_1 = \epsilon_3 = -\nu\epsilon + \alpha\epsilon^2 + \frac{\nu^2}{2}\epsilon^2$$
$$\epsilon_2 = \epsilon + \delta\epsilon^2 + \frac{1}{2}\epsilon^2 \tag{22}$$
$$\epsilon_4 = \epsilon_5 = \epsilon_6 = 0.$$

The application of transverse loading creates birefringence in the optical fibre, resulting in the propagating lightwave dividing into two separately propagating waves, one with a positive phase shift and one with a negative phase shift

$$\Delta\varphi^+ = \left(\frac{\mathrm{d}\varphi}{\mathrm{d}\epsilon}\right)^+\epsilon + \left(\frac{\mathrm{d}^2\varphi}{\mathrm{d}\epsilon^2}\right)\epsilon^2$$
$$\Delta\varphi^- = \left(\frac{\mathrm{d}\varphi}{\mathrm{d}\epsilon}\right)^-\epsilon + \left(\frac{\mathrm{d}^2\varphi}{\mathrm{d}\epsilon^2}\right)\epsilon^2$$
$$\left(\frac{\mathrm{d}\varphi}{\mathrm{d}\epsilon}\right)^+ = \frac{2\pi}{\lambda}Ln_0\left[-\nu - \frac{n_0^2}{2}(p_{11} - 2\nu p_{12})\right]$$
$$\left(\frac{\mathrm{d}\varphi}{\mathrm{d}\epsilon}\right)^- = \frac{2\pi}{\lambda}Ln_0\left[-\nu - \frac{n_0^2}{2}\left(p_{12} - \nu(p_{11} + p_{12})\right)\right] \tag{23}$$
$$\frac{\mathrm{d}^2\varphi}{\mathrm{d}\epsilon^2} = \frac{\pi}{\lambda}Ln_0\left[\alpha - \frac{n_0^2}{2}\left(\left(\delta + \frac{1}{2}\right)p_{11} + (\nu^2 - 2\alpha)p_{12}\right.\right.$$
$$\left.\left. + 4\nu g_{112} - g_{111} - 2\nu^2(g_{123} + g_{122})\right)\right].$$

One observes from (23) that the second-order term for each phase shift is identical. For a more general loading case, the deformation of the optical fibre would have to be derived using the theory of finite elasticity to second order in strain, as the principle of linear superposition cannot be applied to combined loading cases for large deformations [18]. As a final note, the approximations of (18)–(21) for the effect of core radius change on the propagation constant cannot be applied for the transverse loading case, since the cross-section does not remain circular. In section 4 it will be demonstrated that this

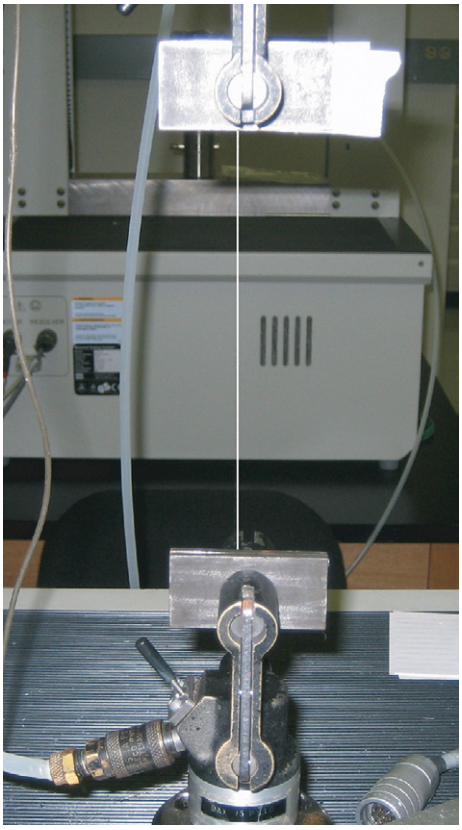

Figure 5. Axial load testing of POF. Location of POF is highlighted with white line (POF is too small to be visible).

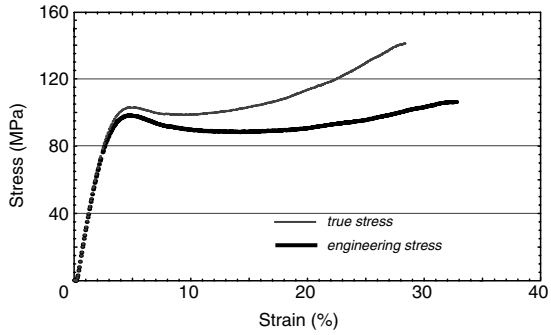

Figure 6. Typical measured stress–strain curve for POF at a strain rate of 0.60 min^{-1}. Both engineering stress and true stress are plotted.

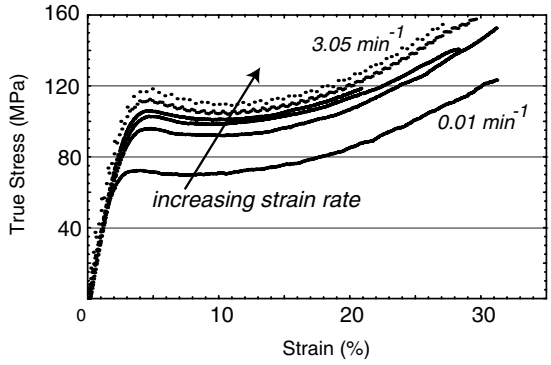

Figure 7. Typical measured true stress–strain curves for POF at various strain rates. Strain rates plotted are 0.01, 0.30, 0.60, 0.90, 1.22 and 3.05 min^{-1}.

does not play a significant role in the response of the sensor for axial loading, therefore we will not further derive this here. However, its effect is expected to be slightly larger for the case of transverse loading.

3. Experimental measurement of mechanical properties

So as to compare the relative importance of the finite deformation for the POF as compared to the silica optical fibre, axial tension tests were performed on PMMA single-mode fibre samples (Paradigm optics: cladding diameter = 125 μm, $a_0 = 3.44$ μm, NA = 0.12). A total of ten samples of length 101 mm were loaded on a Sintech 1/S uniaxial tension machine at a displacement rate of 60 mm min^{-1} (strain rate = 0.60 min^{-1}). Figure 5 shows one fibre sample in the testing machine, held into place with pneumatic grips to prevent large deformation of the fibre at the grips. To determine the effect of strain rate on the mechanical properties of the fibre, three additional specimens per strain rate were tested at strain rates of 0.01, 0.30, 0.90, 1.22 and 3.05 min^{-1}. All samples used in these experiments were from the same batch of POF, to remove variations due to the manufacturing process.

3.1. Stress versus strain response

Throughout each test the axial elongation of the fibre (ϵ_l of (14)) and the applied load were measured. From the load values, both the engineering stress, σ (the ratio of the force and the original area) versus engineering strain and the true stress, σ_t (the ratio of the force and the current area) versus true strain were calculated. The results from a typical fibre at a strain rate of 0.60 min^{-1} are plotted in figure 6. The results were extremely repeatable between specimens and demonstrate the characteristic response of a polymeric material [19]. One can observe the initial linear region of the stress–strain curve until yielding of the fibre, followed by a region of strain softening and finally strain hardening prior to ultimate failure of the fibre at approximately 30% strain. From a sensing perspective the yield strain of the fibre may be a more critical parameter than the ultimate strain as permanent, large deformations in the fibre beyond the yield strain would significantly affect transmission through the fibre. For the current samples, the yield point is around the same value as the ultimate strain for silica fibres, therefore a significant gain in strain range is not apparent. However, it is assumed that with the recent rapid increases in quality of manufacturing for single-mode POFs, the yield point will significantly increase and therefore such a strain range increase will be possible.

Figure 7 plots typical stress versus strain plots for typical specimens measured at different strain rates. From figure 7 we see that the applied strain rate clearly affects the yield point of the POF. As the strain rate increases, the yield strain (and stress) increases as well. On the other hand, the initial response of the POF in the linear region of the curve is less sensitive to strain rate. Therefore, for sensing applications, it is important to know the rate at which strain will be applied to

accurately predict the failure point of the sensor, however less so for the accuracy of the strain prediction itself. The effects of strain rate also are significantly diminished at strain rates above 1 min^{-1}.

3.2. Nonlinear mechanical coefficients

In order to identify the material nonlinear response coefficients E_0 and δ, we follow the procedure of Mallinder and Proctor [20], also used by Bertholds and Dandliker [10]. Assuming that the modulus has the nonlinear form

$$E = \frac{\mathrm{d}\sigma}{\mathrm{d}\epsilon_l} = E_0(1 + \gamma\epsilon_l), \tag{24}$$

where

$$E_0 = \left(\frac{\mathrm{d}\sigma}{\mathrm{d}\epsilon_l}\right)\bigg|_{\epsilon_l=0}, \tag{25}$$

we can solve for the true stress, σ_t,

$$\sigma_t = \int_0^{\epsilon_l} E\,\mathrm{d}\epsilon_l = E_0\left(\epsilon_l + \frac{\gamma}{2}\epsilon_l^2\right). \tag{26}$$

Through (26) and the true stress derived from the axial elongation of (14), one can show that

$$\delta = 2\nu - \gamma/2 \tag{27}$$

which relates the measured γ to the required δ [10]. Equation (27) can be interpreted as the fact that the nonlinearity in the axial elongation of the optical fibre during loading is due to two effects: the reduction in fibre diameter (2ν) and nonlinearities in the material properties ($\gamma/2$).

For each specimen, the curve similar to figure 6 was used to obtain the values of E_0, γ, yield stress and yield strain for the POF. The standard definition of the initial modulus E_0 is the slope of curve evaluated at $\epsilon = 0$ [19] and therefore should be independent of the strain range used for the calculations. However, our goal in this paper is to measure the best fits to the material coefficients for evaluation of (17). In order to do so, we must truncate the polymial fit of the stress–strain curve to only the two terms of (26). Therefore we fix E_0 as the linear coefficient of the second-order polynomial fit to the data and recognize that therefore the calibrated 'material properties' depend upon the strain range at which the sensor is to be applied because we have neglected higher order terms.

The average values obtained for all specimens for each strain range are listed in tables 2 and 3. For some strain rate–strain range combinations, there was not enough nonlinearity in the stress–strain curve to accurately calculate γ, therefore only E_0 is listed. However for most data the correlation, R^2, is also listed and demonstrates that the properties are an excellent fit to the data. The variation in the initial modulus, E_0, and δ with strain range is plotted in figures 8 and 9 for each of the strain rates. The standard deviation between samples is also plotted. As can be seen in figure 8, as the strain range increased, the initial modulus also increased. On the other hand, there is not a clear trend for the nonlinearity, δ, with strain rate (see figure 9). After a maximum strain value between 3 and 4% for each curve, the nonlinearity remains approximately constant whereas E_0 decreases with increasing strain. This will be shown in the following section to be due to yielding of the material.

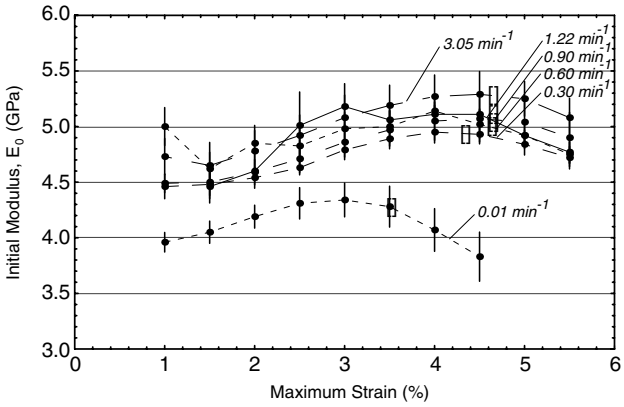

Figure 8. Calculated initial modulus, E_0, plotted as a function of maximum strain considered in the calculation (i.e., for a maximum strain of 2.5%, the strain range considered is 0–2.5%). Values obtained at strain rates of 0.01 to 3.05 min^{-1} plotted. Standard deviation of each point amongst all samples is also indicated. The yield stress for each strain rate curve is indicated as a rectangle (see table 4).

Table 2. Measured and calculated material properties of POF (strain rate from 0.01 to 0.60 min^{-1}). R^2 correlation of curve fit using properties to measured curve is also indicated.

Strain rate	Strain range (%)	E_0 (GPa)	γ	δ	R^2
	0–1.0	3.96	−24.3	12.9	0.9999
	0–1.5	4.05	−26.8	14.1	0.999
	0–2.0	4.19	−29.8	15.6	0.9998
	0–2.5	4.31	−31.7	16.6	0.9998
0.01 min^{-1}	0–3.0	4.34	−32.2	16.7	0.9998
	0–3.5	4.28	−31.6	16.5	0.9996
	0–4.0	4.07	−30.1	15.7	0.9981
	0–4.5	3.83	−28.6	15.0	0.9947
	0–5.0	–	–	–	–
	0–5.5	–	–	–	–
	0–1.0	4.46	−17.0	9.18	0.9999
	0–1.5	4.48	−17.8	9.59	0.9999
	0–2.0	4.54	−19.1	10.2	0.9999
	0–2.5	4.63	−20.6	11.0	0.9999
0.30 min^{-1}	0–3.0	4.79	−22.5	11.9	0.9998
	0–3.5	4.89	−23.4	12.4	0.9998
	0–4.0	4.95	−23.9	12.6	0.9998
	0–4.5	4.93	−23.8	12.6	0.9998
	0–5.0	4.84	−23.3	12.3	0.9995
	0–5.5	4.72	−22.4	11.9	0.9998
	0–1.0	4.05	–	–	–
	0–1.5	3.91	–	–	–
	0–2.0	4.16	−11.5	6.4	0.9989
	0–2.5	4.41	−15.6	8.5	0.9991
0.60 min^{-1}	0–3.0	4.58	−18.4	9.9	0.9992
	0–3.5	4.73	−20.1	10.8	0.9991
	0–4.0	4.85	−21.5	11.4	0.9991
	0–4.5	4.91	−22.0	11.7	0.9991
	0–5.0	5.04	−22.3	11.8	0.9997
	0–5.5	4.90	−21.8	11.6	0.9990

An initial impression of the data in tables 2 and 3 might be that the properties of the fibre vary considerably depending upon the strain range within which one chooses to measure them. However, the curve fits applying these properties do not. To demonstrate this point, curve fits using the properties in table 2 for a strain rate of 60 min^{-1} are plotted in a single

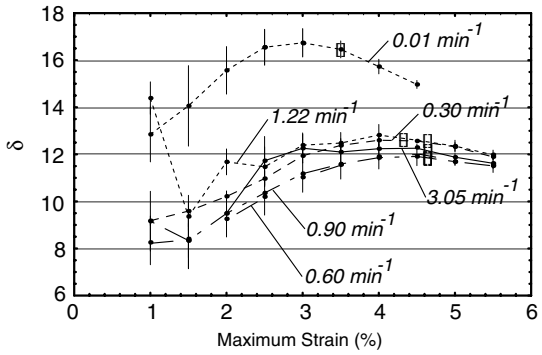

Figure 9. Calculated value of δ, plotted as a function of maximum strain considered in the calculation. Values obtained at strain rates of 0.01 to 3.05 min^{-1} plotted. Standard deviation of each point amongst all samples is also indicated. The yield stress for each strain rate curve is indicated as a rectangle (see table 4).

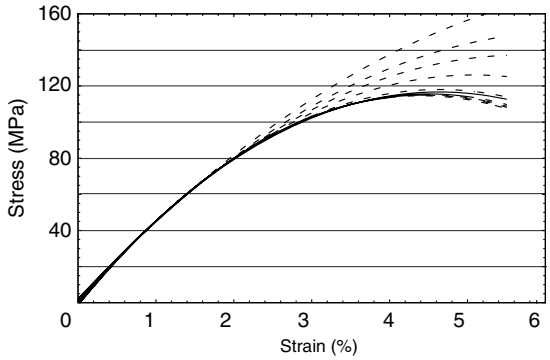

Figure 10. Curve fits to a stress–strain curve using the values of E_0 and γ for a single POF sample at an applied strain rate of 0.60 min^{-1}. Curve fits are plotted for the strain ranges of 0–1.0% to 0–5.5%.

Table 3. Measured material properties of POF (strain rate from 0.90 to 3.05 min^{-1}). R^2 correlation of curve fit using properties to measured curve is also indicated.

Strain rate	Strain range (%)	E_0 (GPa)	γ	δ	R^2
	0–1.0	4.73	−17.0	9.16	0.9998
	0–1.5	4.65	−15.3	8.34	0.9999
	0–2.0	4.78	−17.6	9.49	0.9999
0.90 min^{-1}	0–2.5	4.92	−19.4	10.4	0.9999
	0–3.0	5.08	−21.0	11.2	0.9999
	0–3.5	5.19	−21.8	11.6	0.9998
	0–4.0	5.27	−22.4	11.9	0.9998
	0–4.5	5.29	−22.5	11.9	0.9998
	0–5.0	5.25	−22.0	11.7	0.9997
	0–5.5	5.08	−21.7	11.5	0.9991
	0–1.0	5.00	−27.4	14.4	0.9999
	0–1.5	4.62	−17.4	9.36	0.9996
	0–2.0	4.85	−22.0	11.7	0.9986
1.22 min^{-1}	0–2.5	4.83	−21.6	11.5	0.9997
	0–3.0	4.98	−23.4	12.4	0.9997
	0–3.5	5.00	−23.6	12.5	0.9997
	0–4.0	5.14	−24.3	12.8	0.9997
	0–4.5	5.02	−23.8	12.6	0.9997
	0–5.0	4.92	−23.3	12.4	0.9992
	0–5.5	4.75	−22.6	12.0	0.9899
	0–1.0	–	–	–	–
	0–1.5	4.46	−15.3	8.34	0.9999
	0–2.0	4.59	−17.7	9.50	0.9999
3.05 min^{-1}	0–2.5	5.01	−22.1	11.7	0.9998
	0–3.0	5.12	−23.2	12.3	0.9998
	0–3.5	5.06	−22.9	12.1	0.9998
	0–4.0	5.11	−23.1	12.2	0.9998
	0–4.5	5.11	−23.2	12.3	0.9998
	0–5.0	4.92	−22.4	11.9	0.9989
	0–5.5	4.77	−21.9	11.6	0.9981

graph in figure 10. Each curve is plotted as a solid line for the range over which the parameters apply and as a dashed line beyond the applicable strain range. As can be seen, although the specific values of the parameters vary significantly, the difference in the curve fits is insignificant over the range for which each fit is applicable. A general guideline would then be to use the calibrated parameters of the largest strain range for which the sensor can be applied.

Previously reported values of E_0 for single-mode POFs are typically lower: 2.8 GPa [2] and 2.75 GPa [21], although only the initial portion of the loading curve was used. Using only the initial portion of the curves from the POF samples in this study introduces significantly more variation and yields values of E_0 ranging from 2.8 GPa to 3.4 GPa. It is also difficult to compare between previous studies since the complete stress–strain behaviour of the POF is typically not given, although Jiang *et al* [23] do provide detailed response curves for a PMMA POF. Differences are also expected between different PMMA POFs due to differences in manufacturing processes.

An important difference between the silica optical fibre and the PMMA optical fibre is the magnitude of the nonlinearity due to the material properties, γ. For the PMMA, $\gamma = -22.0$, whereas Bertholds and Dandliker [10] measured a value of $\gamma = 2.2$ for silica. Therefore, the material nonlinearity is an order of magnitude larger for the PMMA, and is of the opposite sign. The importance of this scale will be seen in section 4 in which the sizes of the various effects are compared.

3.3. Yield point

In addition to measuring the material parameters above, it is important to identify the yield point in curves of figure 7. As mentioned above this corresponds to the realistic upper strain limit for application of the sensor. For each of the measured curves, the yield point was calculated using Considere's construction, as commonly applied for polymeric materials [24]. Defining the extension ration, $\lambda_e = \epsilon + 1$, and defining the yield stress as the condition $\mathrm{d}\sigma/\mathrm{d}\epsilon = 0$, it can be shown that the equivalent condition for the true stress, σ_t, is

$$\frac{\mathrm{d}\sigma_t}{\mathrm{d}\lambda_e} = \frac{\sigma_t}{\lambda_e}. \tag{28}$$

From each stress–strain curve, this point is identified by plotting true stress versus extension ratio and drawing a line from the origin to the first tangent of the curve (see inset of figure 11). The intersection point is thus the yield point of the POF.

The stress and strain values at yield were thus determined for each of the measured stress–strain curves. The average calculated value of yield strain and stress for each strain rate is listed in table 4. To show the clear relationship of yield strain on strain rate, the yield strain values are also plotted in

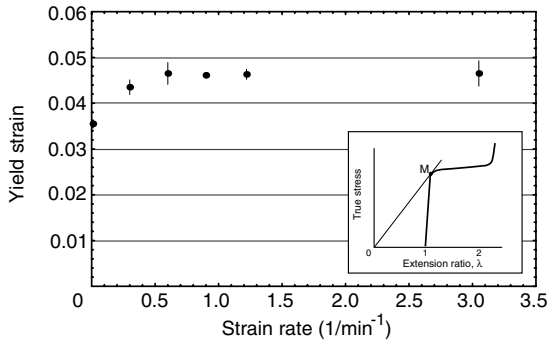

Figure 11. Calculated yield strain versus strain rate for POF samples. Standard deviation amongst samples at each strain rate is also indicated. Inset shows Considere's construction for determination of the yield point.

Table 4. Measured yield strain and stress as a function of strain rate.

Strain rate (min^{-1})	Yield strain (%)	Yield stress (GPa)
0.01	3.55	72.2
0.30	4.35	94.3
0.60	4.65	103.5
0.90	4.61	105.5
1.22	4.63	111.2
3.05	4.65	116.8

figure 11. The asymptotic behaviour of the yield strain as a function of strain rate seen in figure 11 is identical to that measured by Jiang *et al* [23].

Returning to figures 8 and 9, the yield strain of the POF at each strain rate from table 4 has been added to the graphs. One can clearly see that the change in behaviour of the curves for E_0 and δ are due to yielding of the material. For each curve, the decrease in E_0 begins at approximately the yield point. This is also an indication that the form of (24) is less and less applicable as the strain increases beyond the yield point. The fact that the correlation values of the parameter fits in tables 2 and 3 decrease after the yield point confirms this observation.

4. Discussion

The previous sections derived the phase shift of the POF including nonlinear photoelastic effects, finite deformation of the optical fibre, and the resulting core radius change. The third effect is typically neglected for silica fibres at small strains, however it is not apparent whether this assumption still holds for large strains or polymer material properties [12]. The relative magnitude of these effects is investigated in this section for both polymer and silica fibres, using the mechanical properties measured experimentally and presented in the previous section. Since the later nonlinear photoelastic constants have not yet been determined experimentally for the POF, we cannot compare these at this time.

Figure 12 plots the calculated $\Delta\varphi$ for the case of pure axial strain in the range of 0–6% strain. For the silica fibre, typical optical and mechanical properties of a step-index fibre are used, including a failure strain of 5%. As seen in figure 12, the nonlinearity due to the finite deformation becomes significant in the calculation of the sensitivity above approximately 3% strain, at which point the linear and nonlinear curves diverge.

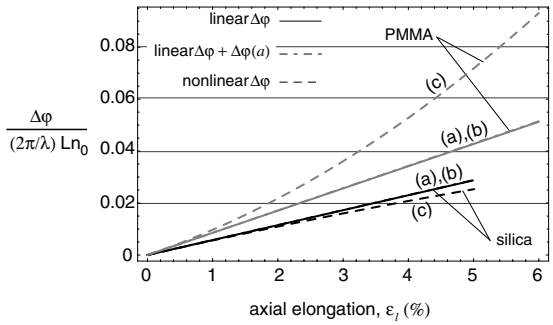

Figure 12. Normalized phase shift of silica optical fibre and POF applying various approximations: linearized Δn_e (see [12]), (*b*) including $(\mathrm{d}n_e/\mathrm{d}a)(\mathrm{d}a/\mathrm{d}\epsilon_0)$ ((19)–(21)), (*c*) including finite deformation of optical fibre ((14)–(15)). Common parameters for optical fibres: $a_0 = 4\ \mu$m, $n_1 = 1.46$, $n_2 = 1.45$, $n_0 = 1.456$, $\lambda = 1550$ nm. Properties of silica [10]: $\nu = 0.16$, $p_{11} = 0.17$, $p_{12} = 0.36$, $\delta = -4.0$, $\alpha = -2.3$, ϵ at failure $= 5\%$. Properties of PMMA [2]: $\nu = 0.34$, $p_{11} = 0.30$, $p_{12} = 0.297$, $\delta = 11.7$ (from table 2), $\alpha = -2.3$.

Additionally, the curve including the effect of the core radius is not distinguishable from the linearized $\Delta\varphi$. Therefore the role of the core radius through (21) can be neglected. The phase shift in a PMMA POF including the linear terms, finite deformation of the optical fibre and the core radius change are also plotted in figure 12 using the same step-index indices of refraction. For these plots, the Pockel's constants and bulk material properties of PMMA were used [2]. The nonlinearity constant δ of 11.6 was used from table 2 corresponding to a strain rate of 0.60 min^{-1} and a strain range of 0–5.5%. Since α was unknown, the same value was applied as for silica. It is expected that the actual value for PMMA is significantly higher (since the value for δ is significantly higher), however changing the value of α did not visibly vary the plots of figure 12.

The salient features of the curves of figure 12 are the following:

(i) The sensitivity of the phase shift in the POF to the applied strain at low strain values is significantly larger than that of the silica fibre. This difference is due to the difference in values of ν, p_{11} and p_{12}. This initial increase in sensitivity was demonstrated experimentally by Silva-Lopez *et al* [2]. From a strain sensing perspective this added sensitivity can be a significant advantage of the POF.

(ii) An important difference between the silica optical fibre and the PMMA optical fibre is the magnitude of the nonlinearity due to the material prosperities, γ. For the PMMA, $\gamma = -22.0$, whereas Bertholds and Dandliker [10] measured a value of $\gamma = 2.2$ for silica. Therefore, the material nonlinearity is an order of magnitude larger for the PMMA, and is of the opposite sign. This difference emphasizes the importance of including the finite deformation effects in POFs, starting at strain magnitudes as low as 1%.

(iii) The strain value at which the nonlinearity must be taken into account is significantly lower for the POF ($\approx$1%) than for the silica fibre ($\approx$3%).

(iv) As for the silica fibre, the curve including the effect of the core radius is not distinguishable from the linearized $\Delta\varphi$

for the PMMA POF. Therefore the core radius change can be neglected even at large strains.

5. Conclusions

In summary, the use of the POF as a sensor to measure large strain magnitudes in structures under general loading conditions requires the calibration of four mechanical parameters (E_0, ν, δ, α) and six opto-mechanical properties (p_{11}, p_{12}, g_{111}, g_{122}, g_{112}, g_{123}). As compared to silica optical fibres, the mechanical nonlinearities in the POF are more significant and are important at strain magnitudes as low as 1%. Measurement of the nonlinear photoelastic properties of the POF will be required before their relative contribution to the phase response is known. The effect of core radius change is not significant in the calculation of the phase response for either the silica or polymer optical fibre. Although the phase shift to strain response is no longer expected to be linear above 1% strain, the large strain to failure capabilities of the POF demonstrate great potential for the measurement of large strain ranges typically observed in structural applications.

Additional effects, such as attenuation with strain of the POF, would limit the range of the data acquisition system used for the sensor and decrease the visibility of an associated interferometer, however will not affect the phase shift. Other potential effects beyond the reach of the current work include the temperature, creep and hysteresis properties of the POF which will likely play a significant role in their long-term response and chromatic dispersion, significant at large strain magnitudes [25]. Finally, the assumption that the POF is mechanically isotropic is not necessarily a good one for POFs. Previous studies have noted that the polymer molecules are aligned in the drawing (axial) direction due to the fabrication process [23]. This alignment of the molecules creates different material properties in the axial and transverse directions. Additionally Dugas and Maurel [26] hypothesized that after the fibre drawing process the PMMA molecular chains tend to move to a more stable equilibrium position through stress relaxation. This stress relaxation causes small cracks to appear in the radial direction. This effect would be further enhanced at elevated temperatures. Dugas and Maurel [26] postulated the existence of such cracks due to the fact the measured attenuation in PMMA fibres was significantly above that of the intrinsic material attenuation of bulk PMMA. In addition to the assumed isotropic mechanical properties, the reduction of the tensor **g** to a function of four independent constants may therefore be an over-simplification of the actual photoelastic effect. A similar comment could be made for the linear photoelastic tensor **p**. With only a few independent calibrations it would be difficult to separate out the individual tensor terms; however future studies may be required to quantify the anisotropy, as well optimize fabrication processes to reduce the effects of the material anisotropy on the sensor response.

Acknowledgment

This work was supported by the National Science Foundation through grant no. CMS 0428301.

References

[1] Kiesel S, Van Vickle P, Peters K, Abdi O, Hassan T and Kowalsky M 2006 Polymer optical fiber sensors for the civil infrastructure *Proc. SPIE Smart Mater. Struct. Symp.* **6174** 996–1007

[2] Silva-Lopez M, Fender A, MacPherson W N, Barton J S, Jones J D C, Zhao D, Dobb H, Webb D J, Zhang L and Bennion I 2005 Strain and temperature sensitivity of a single-mode polymer optical fibre *Opt. Lett.* **30** 3129–31

[3] Xiong Z, Peng G D, Wu B and Chu P L 1999 Highly tunable Bragg gratings in single-mode polymer optical fibers *IEEE Photon. Technol. Lett.* **11** 352–4

[4] Kuang K S C, Akmaluddin Cantwell W J and Thomas C 2003 Crack detection and vertical deflection monitoring in concrete beams using plastic optical fibre sensors *Meas. Sci. Technol.* **14** 205–16

[5] Kuang K S C, Cantwell W J and Scully P J 2002 An evaluation of a novel plastic optical fibre sensor for axial strain and bend measurements *Meas. Sci. Technol.* **13** 1523–34

[6] Takeda N 2002 Characterization of microscopic damage in composite laminates and real-time monitoring by embedded optical fiber sensors *Int. J. Fatigue* **24** 281–9

[7] Kuang K S C and Cantwell W J 2003 The use of plastic optical fibres and shape memory alloys for damage assessment and damping control in composite materials *Meas. Sci. Technol.* **14** 1305–13

[8] Kuang K S C, Cantwell W J and Scully P J 2004 Assessment of an extrinsic polymer-based optical fibre sensor for structural health monitoring *Meas. Sci. Technol.* **15** 2133–41

[9] Van Steenkiste R J and Springer G S 1997 *Strain and Temperature Measurement with fibre Optic Sensors* (Lancaster, PA: Technomic)

[10] Bertholds A and Dandliker R 1987 Deformation of single-mode optical fibers under static longitudinal stress *J. Lightwave Technol.* **5** 895–900

[11] Haslach H W and Sirkis J S 1991 Surface-mounted optical fiber strain sensor design *Appl. Opt.* **30** 4069–80

[12] Butter C D and Hocker G B 1978 Fiber optics strain gauge *Appl. Opt.* **16** 2867–9

[13] Nye J F 1985 *Physical Properties of Crystals: Their Representation by Tensors and Matrices* (Oxford: Oxford Science Publications)

[14] Vedam K and Srinivasan R 1967 Non-Linear piezo-optics *Acta Crystallogr.* **22** 630–4

[15] Ivanov O V and Wang L A 2003 Wavelength shifts of cladding-mode resonance in corrugated long-period fiber gratings under torsion *Appl. Opt.* **42** 2264–72

[16] Nellen P M, Mauron P, Frank A, Sennhauser U, Bohnert K, Pequignot P, Bodor P and Brandle H 2003 Reliability of fiber Bragg grating based sensors for downhole applications *Sensors Actuators* A **103** 364–76

[17] Procopio A T, Zavaliangos A and Cunningham J C 2003 Analysis of the diametrical compression test to the applicability to plastically deforming materials *J. Mater. Sci.* **38** 3629–39

[18] Murhanghan F D 1951 *Finite Deformation of an Elastic Solid* (London: Wiley)

[19] Ehrenstein G W 2001 *Polymeric Materials* (Munich: Hanser) pp 167–213

[20] Mallinder F P and Proctor B A 1964 Elastic constants of fused silica as a function of large tensile strain *Phys. Chem. Glasses* **5** 91–103

[21] Yang D X, Yu J, Tao X and Tam H 2004 Structural and mechanical properties of polymeric optical fiber *Mater. Sci. Eng.* A **364** 256–9

[22] Buck J A 2004 *Fundamentals of Optical Fibers* (London: Wiley) pp 70–71

[23] Jiang C, Kuzyk M G, Ding J-L, Jons W E and Welker D 2002 Fabrication and mechanical behavior of dye-doped polymer optical fiber *J. Appl. Phys.* **92** 4–12

[24] McCrum N G, Buckley C P and Bucknall C B 1997 *Principles of Polymer Engineering* (New York: Oxford University Press) pp 184–9

[25] Simohamed L M, Auguste J L, Rioublanc J, Blondy J M and Reynaud F 1999 Analysis of chromatic dispersion variation in optical fiber under large stretching *Opt. Fiber Technol.* **5** 403–11

[26] Dugas J and Maurel G 1992 Mode-coupling processes in polymethyl methacrylate-core optical fibers *Appl. Opt.* **31** 5069–79